Available online at www.sciencedirect.com
ScienceDirect
Spectrochimica Acta Part A 67 (2007) 719–729
SPECTROCHIMICA ACTA PART A
www.elsevier.com/locate/saa

Nickel(II) complexes of biologically active glutathione: Spectroscopic, kinetics of thermal decomposition and XRPD studies

Bibhesh K. Singh, Parashuram Mishra, Bhagwan S. Garg *

Department of Chemistry, University of Delhi, Delhi 110007, India

Received 23 May 2006; accepted 16 August 2006

Abstract

Nickel(II) complexes of reduced glutathione (GSH) of general composition $Na[Ni(L)(X)]H_2O$, where H_2L = GSH; X = NO_3^-, SCN^-, $CH_3CO_2^-$, Cl^- have been synthesized and characterized by elemental analysis, infrared spectra, electronic spectra, magnetic susceptibility measurements, thermal and X-ray powder diffraction studies. Infrared spectra indicate deprotonation and coordination of cysteinyl sulphur and carboxylate oxygen of glycine residue with nickel ions. It indicates the presence of water molecule in all the complexes which has been supported by TG/DTA. The thermal behavior of complexes shows that water molecule is removed in first step-followed removal of anions and then decomposition of the ligand molecule in subsequent steps. General mechanisms describing the decomposition of the solid complexes are suggested. Kinetic and thermodynamic parameters were computed from the thermal decomposition data. The room temperature magnetic moment values for all the complexes lie in the range of 2.2–2.4 BM, indicating departure from spin only values due to second order Zeeman effect. The electronic spectra indicate planar coordination geometry for all the complexes. Crystal data for $Na[Ni(L)(CH_3CO_2^-)]H_2O$: tetragonal, space group *P*4/*m*, $a = 8.2004$ Å, $b = 8.2004$ Å, $c = 16.0226$ Å, $V = 1077.47$ Å^3, $Z = 2$. Crystal data for $Na[Ni(L)(Cl^-)]H_2O$: cubic, space group *Pm*3, $a = 16.1055$ Å, $b = 16.1055$ Å, $c = 16.1055$ Å, $V = 4178.38$ Å^3, $Z = 6$. Crystal data for $Na[Ni(L)(NO_3^-)]H_2O$: tetragonal, space group *P*4/*m*, $a = 7.2121$ Å, $b = 7.2121$ Å, $c = 12.0200$ Å, $V = 625.22$ Å^3, $Z = 2$.

Keywords: Glutathione; Nickel(II) complexes; Spectra; Thermal studies; X-ray powder diffraction

1. Introduction

Nickel compounds are human carcinogens [1]. Since intracellular Ni(II) is responsible for neoplastic transformation, several divergent concepts in nickel carcinogenesis have been developed [2–4]. Among these, the oxidative concept proposes that Ni(II) complexes formed in vivo in the vicinity of DNA catalyze redox reactions, whose products oxidize DNA. In turn, some of the products of DNA oxidative damage induce mutations, which may lead to neoplastic transformation. Such products include modified bases (primarily 8-oxoguanine), a basic sites (primarily depurinated), base adducts of carbon-centered radicals (including DNA cross-linked proteins), single and double breaks in the phospho-sugar backbone of DNA [2–4]. Alternative mechanisms also explained, e.g. those of inhibition of DNA repair enzymes [5] or alterations of chromatin condensation and/or specific gene expression [6–7]. However, regardless of the actual mechanism(s) of nickel carcinogen sis, the issue of intracellular speciation of Ni(II) ought be considered, to provide a quantitative tool for discrimination between possible and impossible molecular pathways [3]. The intracellular level of reduced GSH is an important factor in cellular resistance to Ni(II), which in turn, depletes cellular GSH stores [8–11].

Glutathione (γ-glu-cys-gly) (Fig. 1) is one of the most abundant small molecules in biosphere. Its main form is the reduced monomer (GSH) serving to detoxicate xenobiotics and heavy metals, reduced protein thiols, maintain cellular membranes and deactivate free radicals [12]. Recently, it is reported to have anticancer activity [13–14] and glutathione enzyme has been used in antineoplastic chemotherapy treatment [15].

Despite much interest in coordination chemistry of GSH [16–20], only little work has been done dealing with Ni–GSH complexation. Because of the presence of potential binding sites in glutathione, its coordination chemistry is complicated and the most definitive information has been obtained by using results from a combination of various techniques. Taking into account the complexity of the process, spectral characterization and the kinetic calculations of all thermal decomposition reaction

* Corresponding author. Tel.: +91 9868359781; fax: +91 2766 6250.
E-mail address: bibheshksingh@yahoo.co.in (B.K. Singh).

1386-1425/$ – see front matter © 2006 Elsevier B.V. All rights reserved.
doi:10.1016/j.saa.2006.08.024

Table 1
Analytical, magnetic and electronic spectral data of the nickel(II)–glutathione complexes

Serial no.	Complexes	Colour	Yield (%)	Analysis found (calculated %)					μ_{eff} (BM)	Electronic spectral data
				C	H	N	S	Ni		
1	$Na[Ni(L)(CH_3CO_2^-)]H_2O$, $[NaNi(C_{12}H_{20}N_3O_9S)]$	Dark brown	76	30.91 (31.01)	4.25 (4.31)	9.00 (9.05)	6.80 (6.89)	12.64 (12.68)	1.95	642, 575, 410, 366
2	$Na[Ni(L)(Cl^-)]H_2O$, $[NaNi(C_{10}H_{17}N_3O_7SCl)]$	Red brown	82	27.04 (27.23)	3.76 (3.86)	9.49 (9.54)	7.20 (7.27)	13.27 (13.37)	2.00	650, 585, 410, 365
3	$Na[Ni(L)(NO_3^-)]H_2O$, $[NaNi(C_{10}H_{17}N_4O_{10}S)]$	Dark brown	80	25.65 (25.70)	3.60 (3.64)	11.84 (11.90)	6.87 (6.85)	12.58 (12.62)	2.10	646, 580, 408, 361
4	$Na[Ni(L)(SCN^-)]H_2O$, $[NaNi(C_{11}H_{17}N_4O_7S_2)]$	Light brown	79	28.38 (28.52)	3.60 (3.67)	12.01 (12.10)	13.76 (13.83)	12.16 (12.20)	1.90	639, 572, 409, 360

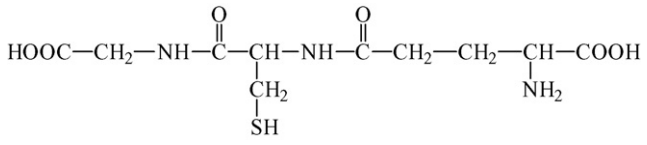

Fig. 1. Structure of glutathione (reduced, GSH).

becomes important tool for the interpretation of structure of complicated molecules. Powder X-ray diffraction has routinely been used as a non-destructive fingerprinting technique in laboratory and industry for several decades. Powder diffraction data is especially useful to deduce accurate cell parameters. The fact that the three-dimensional reciprocal lattice information is condensed onto a one-dimensional intensity profile with respect to 2θ in powder diffraction is the main concern. This leads to overlapping of the diffraction peaks, considerable and preferred orientation among the crystallites.

Therefore, we report herein the synthesis, spectral characterization, magnetic susceptibility measurements, thermal studies and X-ray powder diffraction studies of glutathione with nickel(II) ions.

2. Experimental

Nickel(II) salts and glutathione were procured from Aldrich and were used as received. Solvents used were of analytical grade and were purified by standard methods.

2.1. Preparation of complexes

Glutathione (0.001 M) and sodium hydroxide (0.001 M) were dissolved in water (10 ml) added dropwise in solution of nickel(II) salts (0.001 M) in water (5 ml). There is immediate formation of dark red colour which gradually changes to dark brown solid complexes, these were separated out, which were filtered, washed with water and ethanol and dried over P_4O_{10} in vaccuo.

2.2. Analysis and physical measurements

The stoichiometric analyses (C, H, N, S) were performed using Elementar vario EL III (Germany) model. Metal contents were estimated on a AA-640-13 Shimadzu flame atomic absorption spectrophotometer in solution prepared by decomposing the complex in hot concentrated HNO_3. Infrared spectra were recorded on Perkin-Elmer FT-IR spectrophotometer in KBr and polyethylene pellets. The electronic spectra 900–200 nm of the complexes in solid state was recorded on Jasco-Unidec-430B double beam spectrophotometer. Magnetic susceptibility measurements at room temperature were carried out in powdered state on a vibrating sample magnetometer PAR 155 with 5000G-field strength, using $Co[Hg(SCN)_4]$ (magnetic susceptibility was assumed to be 1.644×10^{-5} cm^3 g^{-1}) as calibrant. Rigaku model 8150 thermoanalyser (Thermaflex) was used for simultaneous recording of TG–DTA curves at a heating rate of 5° min^{-1}. For TG, the instrument was calibrated using calcium oxalate

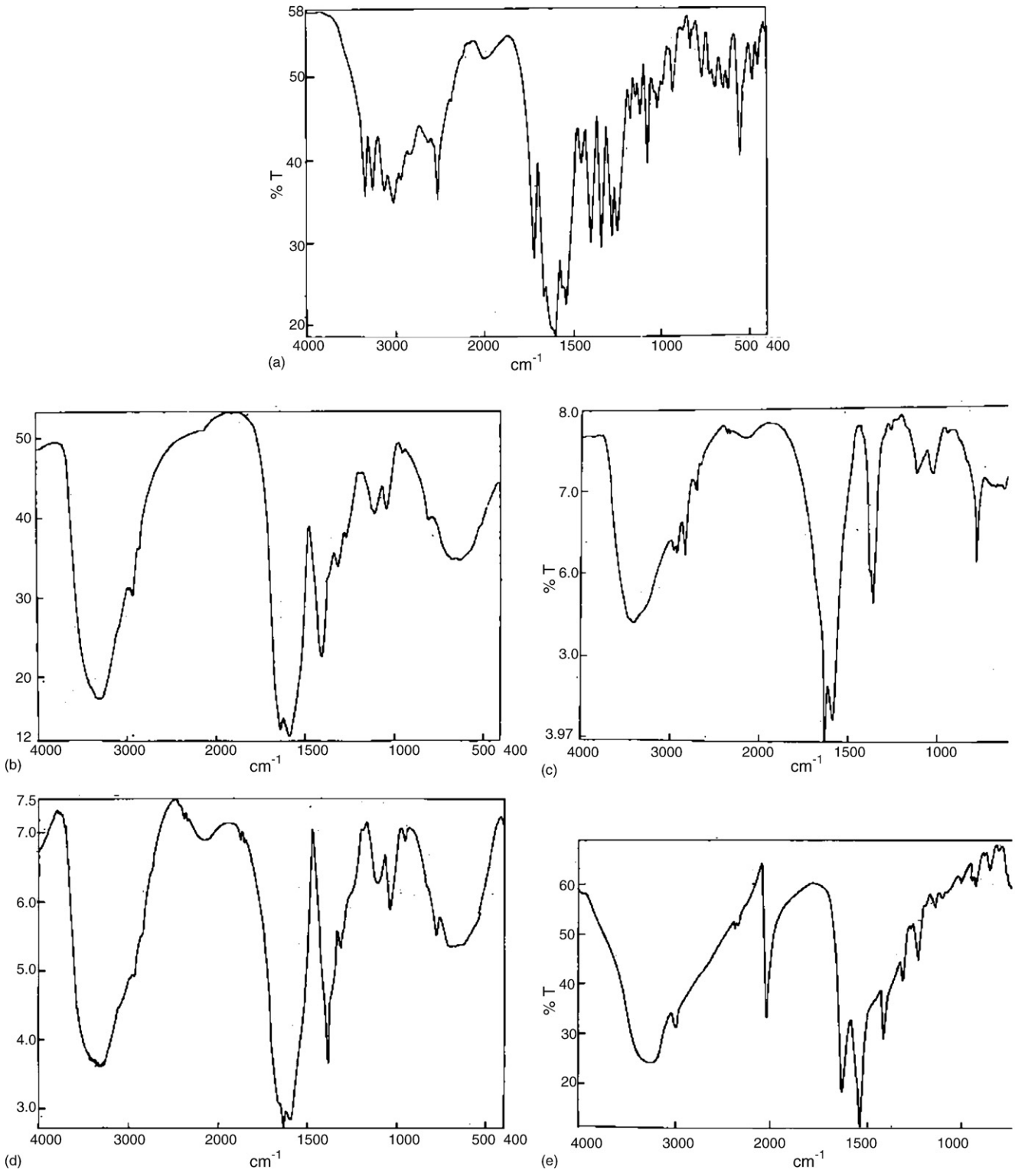

Fig. 2. IR spectrum of: (a) ligand (GSH); (b) $Na[Ni(L)(CH_3CO_2^-)]H_2O$; (c) $Na[Ni(L)(Cl^-)]H_2O$; (d) $Na[Ni(L)(NO_3^-)]H_2O$; (e) $Na[Ni(L)(SCN^-)]H_2O$.

while for DTA, calibration was done using indium metal, both of which were supplied along with the instrument in ambient condition. A flat bed type Al-crucible was used with α-alumina (99% pure) as the reference material for DTA. The number of decomposition steps was identified using TG. The activation energy (E) and Arrhenius constant of the degradation process was obtained by Coats and Redfern method. The XRD powder pattern were recorded on a vertical type Philips 1130/00 X-ray diffractometer, operated at 40 kV and 50 Ma generator using the Cu Kα line at 1.54056 Å as the radiation sources. Each sample were scanned between 10° and 70° (2θ) at 25 °C. The crystallographic data were analyzed by using the CRYSFIRE

Table 2
Infrared spectral data (cm^{-1}) of the GSH (ligand) and their nickel(II) complexes

Serial no.	Compound	ν(OH)	ν(NH)	ν(SH)	ν(C=O)	ν(Ni–S)	ν(Ni–O)	Other assignments
1	GSH	–	3347(s), 3252(s), 3026(s)	2525(s)	1713(s), 1665(w), 1537(m), 1395(s)	–	–	
2	Na[Ni(L)($CH_3CO_2^-$)]H_2O	3485	3326(s, b), 2928(s)	–	1618(s, b), 1585(s), 1395(s)	325	412	
3	Na[Ni(L)(Cl^-)]H_2O	3502	3386(s, b), 2930(m)	–	1632(s), 1580(m), 1362(s)	337	405	388(s) [ν(M–Cl)]
4	Na[Ni(L)(NO_3^-)]H_2O	3513	3333(s, b), 2931(w)	–	1631(s), 1595(s), 1382(s)	331	423	1385, 1276, 1104, 1035, 950, 771, 1766(w), 1754(w)
5	Na[Ni(L)(SCN^-)]H_2O	3454	3312(s, b), 2939(m)	–	1625(s), 1541(s), 1406(s)	322	419	2082(vs), 2062(s), 819(m), 475(m), 272(m)

b: broad, m: medium, s: stronger, vs: very strong, w: weak.

powder indexing software package and the space group was found by GSAS program, density determined by Archimedes method.

3. Results and discussion

GSH reacts with Ni(II) salts in basic medium with the formation of complexes with composition Na[Ni(L)(X)]H_2O (Table 1) where X = $CH_3CO_2^-$, Cl^-, NO_3^-, SCN^- and H_2L = GSH. Complexes were crystalline in nature, insoluble in common organic solvents.

3.1. Infrared spectra and mode of bonding

Glutathione (GSH) is a ligand, which possesses the thiol function, $-COO^-$, NH_2 coordination groups and various forms of GSH deprotonation. The infrared spectral data of the ligand and metal complexes are given in Table 2 and are shown in Fig. 2a–e.

The results indicate that the glutathione shows a strong band at 2525(s) cm^{-1} due to ν(SH), which is absent in the spectra of the complexes indicating the deprotonation and coordination of the thiol group [21]. This has been confirmed by the appearance of ν(Ni–S) band at 340–320 cm^{-1} in all the complexes suggesting the binding of metal through sulphur [22]. In glutathione the band at 1713 cm^{-1} is assigned to the >C=O stretching vibration of the –COOH group of glycine residue, is disappeared, indicating the binding of –COOH group of glycine with metal ions in all the complexes [23]. The band at 1665(m) cm^{-1} in the ligand is assigned to the >C=O stretching of the peptide bonds. This band has been shifted to lower frequency, indicating the coordination of the >C=O group with nickel(II) ion [24]. The doublet peaks, appearing at 3347(s) cm^{-1} and 3252(s) cm^{-1} due to symmetric stretching vibrations of the peptide group [24] merged into a single band in all complexes in the region 3400–3200 cm^{-1}. The peak appearing at 3026(s) cm^{-1} in the free ligand is due to the N–H stretching in a hydrogen bonded NH_3^+ in zwitter ion $^-OOC–C–NH_3^+$ of the amino acid moiety [25]. This band does not show any considerable shift, indicating the non-participation in complex formation. A broad diffused band 3400–3500 cm^{-1} may be assigned to ν(OH) for lattice H_2O in complexes [26]. This band is absent in the ligand.

The >C=O and C–O stretching frequency at 1537(m) cm^{-1} and 1396(s) cm^{-1} in glutathione are assigned to $\nu_{as}(CO_2)$ and $\nu_s(CO_2)$ modes of the carboxylate group and these bands shows considerable shift in all the complexes [27,28].

In addition to the ligand bands modified slightly on account of coordination, infrared spectra of the nickel nitrate complex with glutathione show absorption bands at ca. 1276, 1104, 771, 1385, 950, 1035 cm^{-1} due to coordinated nitrato groups. These bands are assigned as ν_1, ν_2, ν_3, ν_4, ν_5, ν_6 modes, respectively, and their frequencies are consistent with those associated with terminally bonded monodentate nitrato groups [29,30]. In addition to these, two weak bands with a separation of ca. 12 cm^{-1} appear in the 1800–1700 cm^{-1} region indicating clearly the exclusive presence of terminal monodentate nitrato groups [31,32].

In acetato complex, band at 1618 and 1395 cm^{-1} can be assigned to $\nu_{as}(CO_2)$ and $\nu_s(CO_2)$ fundamental stretching bands,

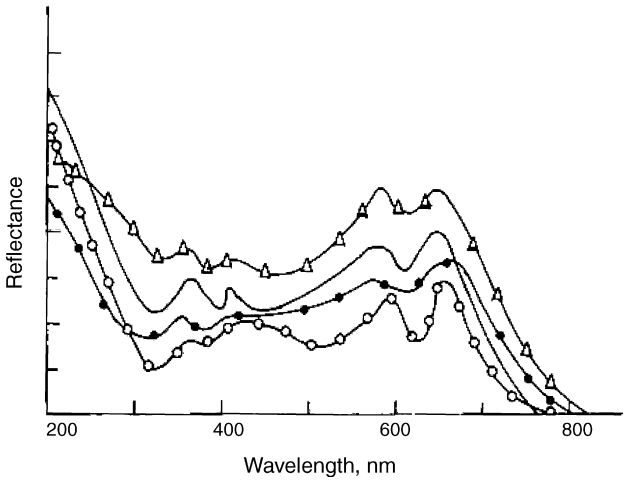

Fig. 3. Electronic spectra of complexes. (a) $Na[Ni(L)(CH_3CO_2^-)]H_2O$ (—); (b) $Na[Ni(L)(Cl^-)]H_2O$ (◯); (c) $Na[Ni(L)(NO_3^-)]H_2O$ (●); (d) $Na[Ni(L)(SCN^-)]H_2O$ (△).

respectively, which are in agreement with the acetate group being monodentate [22,27] because the difference is 223 cm^{-1}. The band at 1395 cm^{-1} is due to $\nu_{as}(CO_2)$ mode of both acetate and ligand. In chloro complex, ν(M–Cl) band is observed at 388 cm^{-1}, which showed terminal rather than bridging chlorine [33].

In the complex with NCS^- group, it seems to be that NCS^- coordinated through the nitrogen atom since ν(C≡N), ν(C–S) and δ(NCS) are observed, respectively, in regions of 2090–2060 cm^{-1}, 830–810 cm^{-1}, 490–470 cm^{-1}, respectively [34]. In this case Ni–N stretching vibration observed at 272 cm^{-1}.

3.2. Magnetic susceptibility and electronic spectra

As further structural tools, magnetic and solid reflectance spectral studies have been used to confirm the geometry of the complexes. The magnetic susceptibility measurements were carried out in the solid state at 25 °C. The results are presented in Table 1. Magnetic moments for the nickel(II) complexes lies in the range 2.2–2.4 BM, is lower than that octahedral, tetrahedral or high spin five coordinate complex, suggesting square planar geometry. The reason for the departure from the spin only value lies partly in the existence of the second order Zeeman effect between the ground and the higher ligand field terms [35]. However, it lies mainly in the fact, that in the presence of spin–orbit coupling, the quenching effect of the ligand field cannot be complete. The electronic spectra of the complexes are listed in Table 1. The spectrum of the complexes (Fig. 3a–d) shows, absorption bands in the visible region 650–635 nm and 590–570 nm may be assigned to the $^1A_{1g} \rightarrow {}^1A_{2g}$ and $^1A_{1g} \rightarrow {}^1B_{1g}$ transitions, respectively, which are consistent with a square planar stereochemistry with the nickel(II) ions [36,37]. The band at region 410–408 nm, 365–360 nm are due to charge transfer spectra from the transition E + Sπx → Ni and Sπx → Ni, respectively, where E is irreducible representation of d–d transition, i.e., $d_{xz,yz} \rightarrow d_{x^2-y^2}$ and Sπx → Ni is charge transfer band from π sulphur orbital to Ni(II).

3.3. Thermo analytical studies

The correlations between the different decomposition steps of the ligand/complexes with the corresponding weight losses are discussed in terms of the proposed formula of the ligand/complexes.

The ligand glutathione (GSH) (Fig. 4a) with the general formula ($C_{10}H_{17}N_3O_6S$) is thermally decomposed in two successive steps. The first decomposition step of estimated mass loss 34.90% (calculated mass loss = 35.00%) within the temperature range 465–505 K may be attributed to the liberation of $2CO_2 + NH_3$. The DTA curve gives endothermic peak at 488 K (maximum peak temperature). The second step occurs within the temperature range 650–810 K with the estimated mass loss 50.10% (calculated mass loss = 50.51%) are reasonably accounted for the decomposition of the rest of the molecule. The DTA curve gives broad diffused exothermic peak at 729 K (maximum peak temperature). The ligand is completely decomposed at temperature 825 K.

The $Na[Ni(L)(CH_3CO_2^-)]H_2O$ complex (Fig. 4b) with the general formula $Na[Ni(C_{12}H_{18}N_3O_8S)]H_2O$ was thermally decomposed in three successive decomposition steps. The first decomposition step of estimated mass loss 4.00% (calculated mass loss = 3.87%) is due to the elimination of one water molecule in the temperature range 327–383 K. This dehydration range indicates the presence of non-coordinated water molecule in the complex. Infrared studies and the endothermic peak at 369 K (maximum peak temperature) by DTA curve also confirm this fact. The second step occurs within the temperature range 553–588 K with the estimated mass loss 16.25% (calculated mass loss 16.60%) may be attributed to the loss of acetate (as CH_4 and CO_2 gases) and NH_3 molecule of the ligand. The DTA curve gives endothermic peak at 574 K (maximum peak temperature). The third step of decomposition occurs within the temperature range 723–833 K with an estimated mass loss 53.05% (calculated mass loss = 52.92%) which corresponds to the loss of $C_9H_{11}NO_5S$ molecule of the ligand leaving NiO + NaCN residue with a total estimated mass loss 73.30% (total calculated mass loss = 73.39%). The end product (residue) was confirmed by comparing observed and calculated mass of pyrolysis product. The DTA curve shows exothermic peak at 797 K (maximum peak temperature).

The $Na[Ni(L)(Cl^-)]H_2O$ complex (Fig. 4c) with the general formula, $Na[Ni(C_{10}H_{15}N_3O_6SCl)]H_2O$ was thermally decomposed in three successive steps. The thermogravimetric decomposition pattern indicates the loss of lattice water also seen as in endothermic peak in the DTA in the 330–390 K ranges. This factor is further confirmed by infrared studies. The first estimated loss is 3.80% (calculated mass loss = 4.10%). The second step occurs within the temperature range 550–613 K with an estimated mass loss of 22.00% (calculated mass loss = 22.08%) which corresponds to the loss of $HCl + NH_3 + CO_2$ molecule. The DTA curve gives endothermic peak at 574 K (maximum

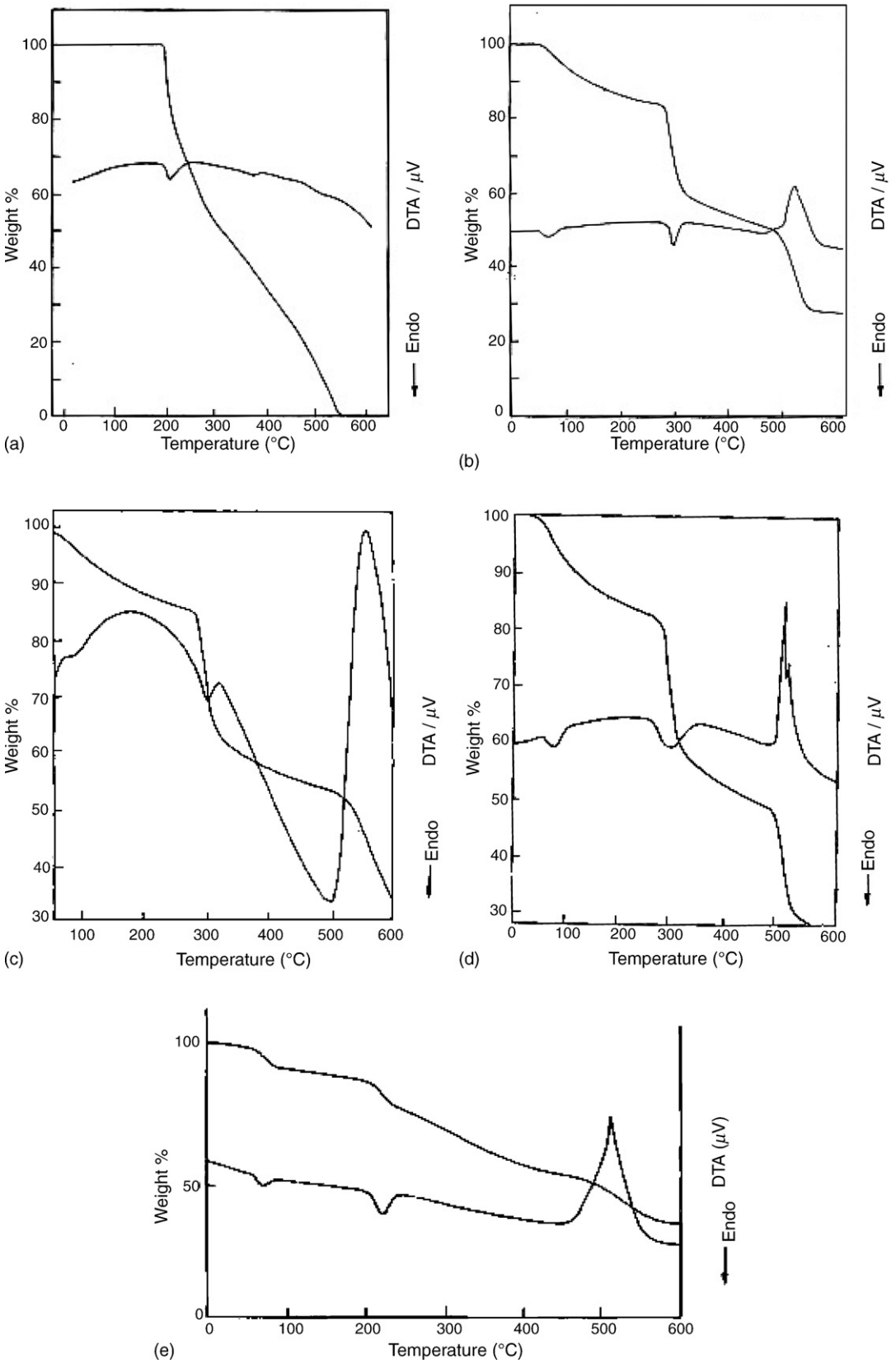

Fig. 4. TG/DTA curves of: (a) ligand (GSH); (b) $Na[Ni(L)(CH_3CO_2^-)]H_2O$; (c) $Na[Ni(L)(Cl^-)]H_2O$; (d) $Na[Ni(L)(NO_3^-)]H_2O$; (e) $Na[Ni(L)(SCN^-)]H_2O$.

peak temperature). The third step involves the decomposition of the remaining ligand $C_8H_{11}NO_3S$ with an estimated mass loss 49.32% (calculated mass loss = 49.00%) in the 773–870 K range within the possibility of formation of nickel oxide and sodium cyanide as end product. The end product (residue) was confirmed by comparing observed and calculated mass of pyrolysis product. The DTA curve gives exothermic peak at 821 K (maximum peak temperature).

The $Na[Ni(L)(NO_3^-)]H_2O$ complex (Fig. 4d) with the general formula, $Na[Ni(C_{10}H_{15}N_4O_9S)]H_2O$ was thermally decomposed again in three stages. The first estimated mass loss of 16.98% (calculated mass loss = 17.09%) within the temperature range 330–400 K could be attributed to the liberation of nitrate group as $(NO_2 + (1/2)O_2)$ gases along with H_2O molecule. The DTA curve gives endothermic peak at 365 K (maximum peak temperature). The second step occurs within the temperature range 523–613 K with an estimated mass loss 23.22% (calculated mass loss 22.44%), which is reasonably accounted for the loss of $NH_3 + 2CO_2$ molecule. The DTA curve gives endothermic peak at 578 K (maximum peak temperature). The third step occurs within the temperature733–853 K, with an estimated mass loss 32.85% (calculated mass loss = 34.00%) are reasonably accounted for the decomposition of the remaining part of the ligand molecule ($C_9H_{12}NO_5S$) leaving nickel oxide and sodium cyanide as residue. The total estimated mass loss 73.05% (total calculated mass loss = 73.53%). The end product (residue) was confirmed by comparing observed and calculated mass of pyrolysis product. The DTA curve gives exothermic peak at 788 K (maximum peak temperature).

The $Na[Ni(L)(SCN^-)]H_2O$ complex (Fig. 4e) with the general formula, $Na[Ni(C_{11}H_{15}N_4O_6S_2)]H_2O$ was thermally decomposed in three steps. The first estimated mass loss 3.80% (calculated mass loss 3.88%) within the temperature range 320–361 K can be attributed to the liberation of water molecule. The DTA curve gives endothermic peak at 348 K (maximum peak temperature). The second step occurs within the temperature range 470–511 K with an estimated mass loss 21.45% (calculated mass loss = 20.90%) which is reasonably accounted for the loss of $CH_4 + SO_2 + NH_3$ molecule. The DTA curve gives endothermic peak at 495 K (maximum peak temperature). The third step occurs within the temperature range 525–836 K with an estimated mass loss 49.23% (calculated mass loss = 48.26%), which is reasonably accounted for the loss of rest of the ligand molecule ($C_9H_8N_2O_3S$), leaving NiO + NaCN as residue with total estimated mass loss 74.48% (total calculated mass loss = 73.04%). The end product (residue) was confirmed by comparing observed and calculated mass of pyrolysis product. The DTA curve gives exothermic peak at 790 K (maximum peak temperature).

Accordingly, to these conclusions, the decomposition mechanisms proposed for glutathione and these complexes are summarized as follows

1. $C_{10}H_{17}N_3O_6S \xrightarrow{488\,K} 2CO_2 + NH_3 + C_8H_{14}N_2O_2S, C_8H_{14}N_2O_2S \xrightarrow{729\,K} C_3H_8 + 5C + 2NH_3 + SO_2$
2. $Na[Ni(C_{12}H_{18}N_3O_8S)]H_2O \xrightarrow{369\,K} H_2O + Na[Ni(C_{12}H_{18}N_3O_8S)]$,
   $Na[Ni(C_{12}H_{18}N_3O_8S)] \xrightarrow{574\,K} CH_4 + CO_2 + NH_3 + C_{10}H_{11}N_2O_6SNaNi$,
   $C_{10}H_{11}N_2O_6SNaNi \xrightarrow{797\,K} C_9H_{11}NO_5S + NiO + NaCN$
3. $Na[Ni(C_{10}H_{15}N_3O_6SCl)]H_2O \xrightarrow{372\,K} H_2O + Na[Ni(C_{10}H_{15}N_3O_6SCl)]$,
   $Na[Ni(C_{10}H_{15}N_3O_6SCl)] \xrightarrow{574\,K} HCl + NH_3 + CO_2 + C_9H_{11}N_2O_4SNaNi$,
   $C_9H_{11}N_2O_4SNaNi \xrightarrow{821\,K} C_8H_{11}NO_3S + NiO + NaCN$
4. $Na[Ni(C_{10}H_{15}N_4O_9S)]H_2O \xrightarrow{365\,K} H_2O + NO_2 + \frac{1}{2}O_2 + Na[Ni(C_{10}H_{15}N_3O_6S)]$,
   $Na[Ni(C_{10}H_{15}N_3O_6S)] \xrightarrow{578\,K} 2CO_2 + NH_3 + C_8H_{12}N_2O_2SNaNi$,
   $C_8H_{12}N_2O_2SNaNi \xrightarrow{788\,K} C_7H_{12}NOS + NiO + NaCN$
5. $Na[Ni(C_{11}H_{15}N_4O_6S_2)]H_2O \xrightarrow{348\,K} H_2O + Na[Ni(C_{11}H_{15}N_4O_6S_2)]$,
   $Na[Ni(C_{11}H_{15}N_4O_6S_2)] \xrightarrow{465\,K} CH_4 + SO_2 + NH_3 + Na[Ni(C_{10}H_8N_3O_4S)]$,
   $Na[Ni(C_{10}H_8N_3O_4S)] \xrightarrow{790\,K} C_9H_8N_2O_3S + NiO + NaCN$

3.4. Kinetics of thermal decomposition

The two stages of decomposition of the ligand and three-stage decomposition of the complexes were studied in more detail. In recent years there has been increasing interest in determining the rate-dependent parameters of solid-state non-isothermal decomposition reactions by analysis of TG curves. Several equations [38–44] have been proposed as means of analyzing a TG curve and obtaining values for kinetic parameters. Many authors [38–42] have discussed the advantage of this method over the conventional isothermal method. The rate of a decomposition process can be described as the product of two separate functions of temperature and conversion [39], using

$$\frac{d\alpha}{dt} = k(T) f(\alpha) \quad (1)$$

where α is the fraction decomposed at time t, $k(T)$ is the temperature-dependent function and $f(\alpha)$ is the conversion function dependent on the mechanism of decomposition. It has been established that the temperature-dependent function $k(T)$ is of the Arrhenius type and can be considered as the rate

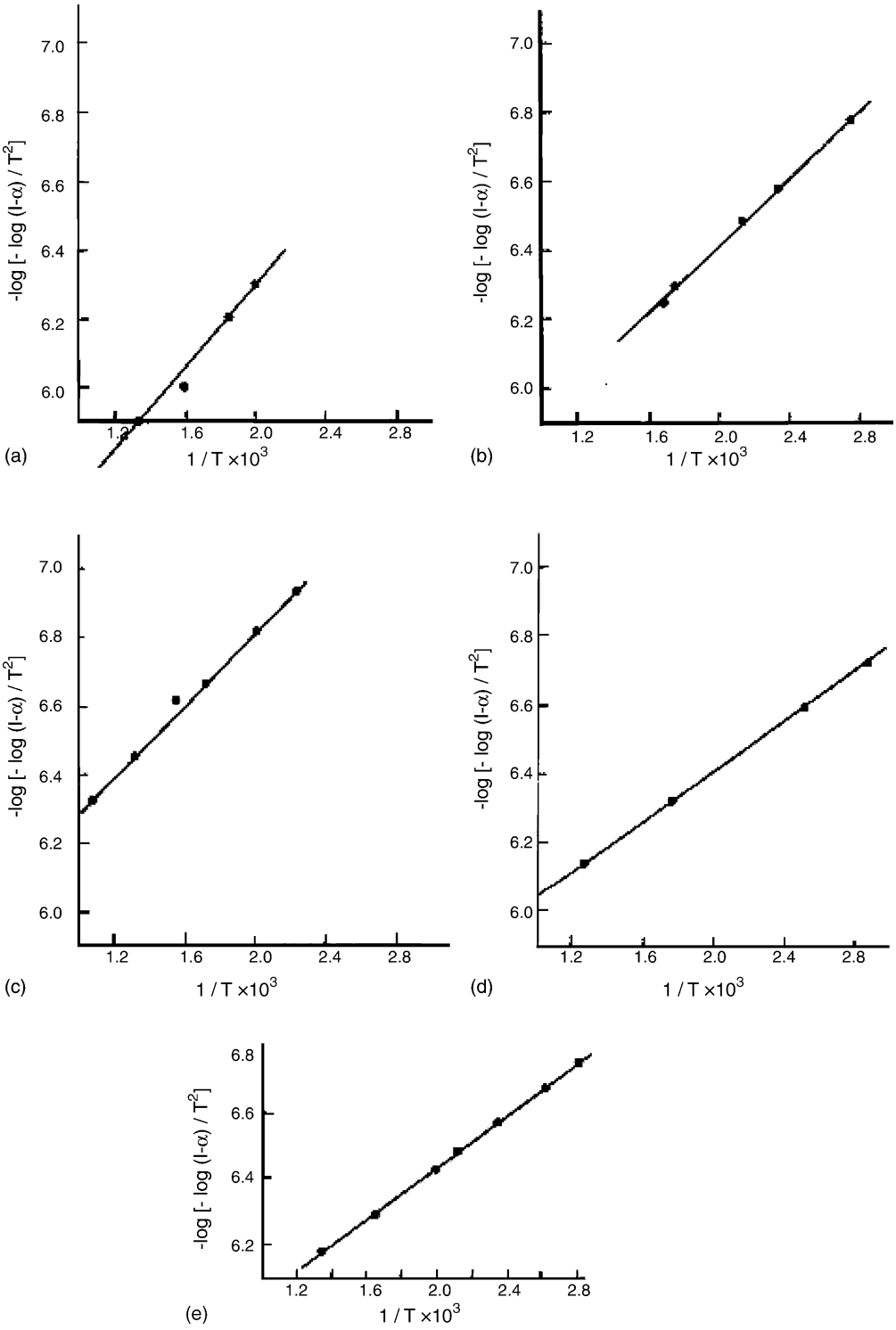

Fig. 5. Linearization plot of: (a) ligand (GSH); (b) Na[Ni(L)($CH_3CO_2^-$)]H_2O; (c) Na[Ni(L)(Cl^-)]H_2O; (d) Na[Ni(L)(NO_3^-)]H_2O; (e) Na[Ni(L)(SCN^-)]H_2O.

constant k:

$$k = A\,\mathrm{e}^{E^*/RT} \tag{2}$$

where R is the gas constant in ($\mathrm{kJ\,deg^{-1}\,mol^{-1}}$). Substituting Eq. (2) into Eq. (1), we get

$$\frac{\mathrm{d}\alpha}{\mathrm{d}t} = \frac{A}{\theta\,\mathrm{e}^{E^*/RT}}\,f(\alpha) \tag{3}$$

where θ is the linear rate $\mathrm{d}T/\mathrm{d}t$. On integration and approximation, this equation can be obtained in the following form

$$\log g(\alpha) = -\frac{2.303E^*}{RT} + \log\left[\frac{AR}{\theta E^*}\right] \tag{4}$$

where $g(\alpha)$ is a function of α dependent on the mechanism of the reaction. The integral on the right hand side is known as temperature integral and has no closed for solution. So several

Table 3
Thermodynamic activation parameters

Serial no.	Compound	Order (n)	E^* (J mol^{-1})	A ($\times 10^5$ s^{-1})	ΔS^* (J K^{-1} mol^{-1})	ΔH^* (J mol^{-1})	ΔG^* (kJ mol^{-1})
1	GSH	1	31.28	0.36	−161.43	53.24	78.99
			32.86	0.27	−167.25	431.45	122.27
2	Na[Ni(L)($CH_3CO_2^-$)]H_2O	1	38.23	1.23	−148.99	68.78	55.05
			52.56	1.49	−170.70	70.16	98.05
			57.34	1.27	−155.08	1297.84	124.90
3	Na[Ni(L)(Cl^-)]H_2O	1	34.75	2.25	−144.05	29.39	53.63
			36.32	1.59	−150.53	45.62	86.43
			38.23	1.23	−155.63	957.97	128.79
4	Na[Ni(L)(NO_3^-)]H_2O	1	49.15	2.64	−142.59	88.22	52.28
			51.25	1.81	−149.53	75.93	119.09
			58.49	1.73	−152.47	1110.58	121.41
5	Na[Ni(L)(SCN^-)]H_2O	1	49.56	2.79	−140.98	45.32	49.11
			50.95	2.04	−147.31	68.26	72.99
			46.32	1.54	−161.46	874.86	128.43

techniques have been used for the evaluation of temperature integral. Most commonly used methods for this purpose are the differential method of Freeman and Carroll [38], integral method of Coats and Redfern [40], the approximation method of Horowitz and Metzger [43]. The kinetic parameters calculated by the Horowitz–Metzger method revealed no significant difference with that evaluated by the Coats–Redfern method. So integral method of Coats–Redfern and using this method various kinetic parameters calculated is discussed here in detail.

The kinetic analysis parameters such as activation energy (ΔE^*), enthalpy of activation (ΔH^*), entropy of activation (ΔS^*), free energy change of decomposition (ΔG^*) were evaluated graphically by employing the Coats–Redfern relation (5):

$$\log\left[-\frac{\log(1-\alpha)}{T^2}\right] = \log\left[\frac{AR}{\theta E^*(1-2RT/E^*)}\right] - \frac{E^*}{2.303RT} \quad (5)$$

where α is the mass loss up to the temperature T, R the gas constant, E^* the activation energy in J mol^{-1}, θ the linear heating rate and $(1-2RT/E^*) \cong 1$. A plot of left hand side of Eq. (5) against $1/T$ gives a slope from which E^* was calculated and A (Arrhenius constant) was determined from the intercept. From relevant data, linearization plots have been drawn in Fig. 5a–d confirms first order kinetics. It has been found that E^* values for complexes > ligand .The calculation of heat of reaction (ΔH^*) (Table 4) from the DTA curves were done by using relation (6):

$$\Delta H^* \,(\mathrm{J\,mol^{-1}}) = \Delta H\,(\mathrm{muv}) \times 60 \times 10^{-6} M \quad (6)$$

where M is the molar mass of the complex and muv = micro unit volt. The entropy of activation (ΔS^*) and the free energy change of activation (ΔG^*) were calculated using Eqs. (7) and (8):

$$\Delta S^* \,(\mathrm{J\,K^{-1}\,mol^{-1}}) = 2.303R\left[\log\left(\frac{Ah}{kT}\right)\right] \quad (7)$$

$$\Delta G^* \,(\mathrm{J\,mol^{-1}}) = \Delta H^* - T\Delta S^* \quad (8)$$

where k and h are the Boltzman and Plank constant, respectively. The calculated values of E^*, A, ΔS^*, ΔH^* and ΔG^* for the decomposition steps of the ligand and complexes are given in Table 3. According to the kinetic data obtained from the TG curves, all the complexes have a negative entropy, which indicates that the complexes are formed spontaneously. The negative entropy also indicates a more ordered activated state that

Table 4
Crystal data of metal complexes

Empirical formula	$NaNiC_{12}H_{20}N_3O_9S$	$NaNiC_{10}H_{17}N_3O_7SCl$	$NaNiC_{10}H_{17}N_4O_{10}S$
Formula weight	464.05	440.46	467.01
Temperature (K)	298	298	298
Wave length (Å)	1.54056	1.54056	1.54056
Crystal system	Tetragonal	Cubic	Tetragonal
Space group	$P4/m$	$Pm3$	$P4/m$
Unit cell dimensions	$a = 8.200418$ Å, $b = 8.200418$ Å, $c = 16.022610$ Å, $\alpha = \beta = \gamma = 90^\circ$	$a = 16.1055$ Å, $b = 16.1055$ Å, $c = 16.1055$ Å, $\alpha = \beta = \gamma = 90^\circ$	$a = 7.212145$ Å, $b = 7.212145$ Å, $c = 12.0200$ Å, $\alpha = \beta = \gamma = 90^\circ$
Volume (Å^3)	1077.47	4178.38	625.22
2θ range	12.18–44.91	23.00–58.67	16.00–65.00
Limiting indices	$0 \le h \le 3$, $0 \le k \le 1$, $1 \le l \le 7$	$3 \le h \le 10$, $1 \le k \le 6$, $3 \le l \le 10$	$2 \le h \le 8$, $1 \le k \le 8$, $0 \le l \le 2$
Density (g/cm^3)	1.43	1.045	2.48
Z	2	6	2
R_f	0.0000846	0.000016	0.0000696

may be possible through the chemisorption of oxygen and other decomposition products. The negative values of the entropies of activation are compensated by the values of the enthalpies of activation, leading to almost the same values for the free energies of activation [17].

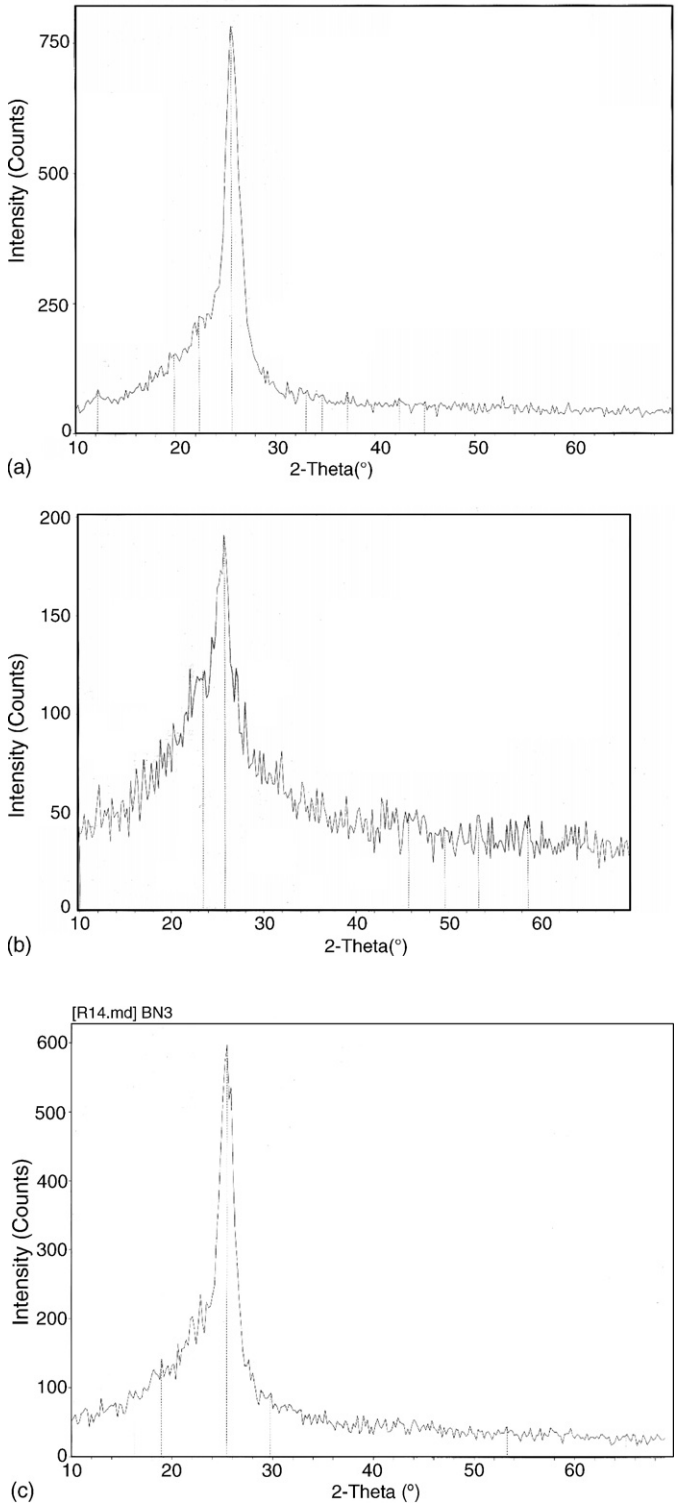

Fig. 6. X-ray diffraction of: (a) $Na[Ni(L)(CH_3CO_2^-)]H_2O$; (b) $Na[Ni(L)(Cl^-)]H_2O$; (c) $Na[Ni(L)(NO_3^-)]H_2O$.

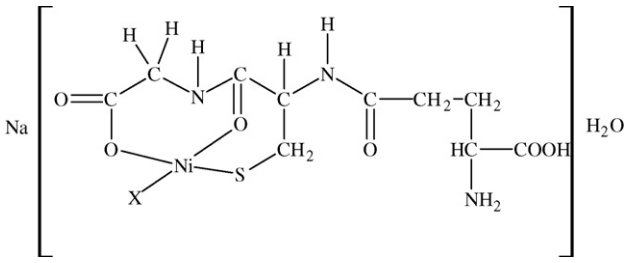

Fig. 7. Proposed structure for $Na[Ni(L)(X)]H_2O$ complexes, where $X = CH_3CO_2^-$, Cl^-, NO_3^-, SCN^- and H_2L = GSH.

3.5. X-ray powder diffraction studies

Structure determination by X-ray powder diffraction data has gone through a recent surge since it has become important to get to the structural information of materials, which do not yield good quality single crystals. The indexing procedures were performed using (CCP_4, UK) CRYSFIRE program [45] giving tetragonal crystal system for $Na[Ni(L)(CH_3CO_2^-)]H_2O$ (Fig. 6a) having M(9) = 14, F(9) = 7, cubic crystal system for $Na[Ni(L)(Cl^-)]H_2O$ (Fig. 6b) having M(6) = 16, F(6) = 6and tetragonal crystal system for $Na[Ni(L)(NO_3^-)]H_2O$ (Fig. 6c) having M(6) = 23, F(6) = 9, as the best solutions. Their cell parameters are shown in Table 4.

Thus on the basis of the above physico-chemical data in conjunction with consideration of ring strain the proposed square planar structure of the complexes is shown in Fig. 7.

4. Conclusion

Nickel(II) complexes were found to be monomer and involved coordination through cystein sulphur and carboxylate oxygen giving square planar geometry. Infrared spectra indicate the presence of H_2O molecule in the complexes that has been supported by TG/DTA. Kinetic studies shows the decomposition follows first order kinetics and proceeds in three-step decomposition. Magnetic susceptibility measurements and electronic spectra also support square planar coordination geometry for all the complexes. The complex crystallizes in the tetragonal/cubic crystal system.

Acknowledgement

B.K. Singh is thankful to University Grants Commission, New Delhi, India for financial assistance under research award scheme.

References

[1] International Agency for Research on Cancer (IARC), Monographs on the Evaluation of Carcinogenic Risk to Humans, vol. 49, Lyon, 1990, p. 257.
[2] K.S. Kasprzak, G.S. Buzard, in: J. Koropatnick, R. Zalups (Eds.), Molecular Biology and Toxicology of Metals, Taylor and Francis, London, 2000, p. 477.
[3] W. Bal, H. Kozlowski, K.S. Kasprzak, J. Inorg. Biochem. 79 (2000) 213.
[4] W. Bal, K.S. Kasprzak, Toxicol. Lett. 127 (2002) 55.
[5] A. Hartwig, T. Schwerdtle, Toxicol. Lett. 127 (2002) 47.
[6] E. Denkhaus, K. Salnikow, Crit. Rev. Oncol. Hematol. 42 (2002) 35.

[7] H. Cangul, L. Broday, K. Salnikow, J. Sutherland, W. Peng, Q. Zhang, V. Poltaratsky, H. Yee, M.A. Zoroddu, M. Costa, Toxicol. Lett. 127 (2002) 69.
[8] W. Li, Y. Zhao, I.N. Chou, Toxicology 77 (1993) 65.
[9] S. Lynn, F.H. Yew, J.W. Hwang, M.J. Tseng, K.Y. Jan, Carcinogenesis 15 (1994) 2811.
[10] W. Li, Y. Zhao, I.N. Chou, Toxicol. Appl. Pharmacol. 136 (1996) 101.
[11] K. Salnikow, M. Gao, V. Voitkun, X. Huang, M. Costa, Cancer Res. 54 (1994) 6407.
[12] K. Arthur, B. Wojciech, Bioinorg. Chem. Appl. 2 (2004) 293.
[13] K.P. Rice, P.G. Penkth, S. Krishnamurthy, A.C. Sartorelli, Biochem. Pharmacol. 69 (2005) 1463.
[14] W.H. Ang, I. Khalaida, C.S. Allardycel, L. Juillerat-Jeanneret, P.J. Dyson, J. Am. Chem. Soc. 127 (2005) 1382.
[15] Z. Kopamski, M. Grabowska, A. Kosiniak-Kamysz, J. Brtrandt, L. Kolodziejski, W. Opoka, M. Schlegel-Zawadzka, Biofactors 22 (2004) 79.
[16] B.K. Singh, R.K. Sharma, B.S. Garg, Spectochim. Acta A 63 (2006) 97.
[17] B.K. Singh, R.K. Sharma, B.S. Garg, J. Therm. Anal. Calorim. 84 (2006) 593.
[18] D.N. Kumar, B.K. Singh, B.S. Garg, P.K. Singh, Spectochim. Acta A 59 (2003) 1487.
[19] K. Arthur, S. Wojciech, S. Magdalena, J.B. Malgorzata, B. Wojciech, Chem. Res. Toxicol. 16 (2003) 855.
[20] P.K. Singh, B.S. Garg, D.N. Kumar, B.K. Singh, Ind. J. Chem. A 40 (2001) 1339.
[21] J. Silver, M.Y. Hamed, I.E.G. Morrison, Inorg. Chim. Acta 107 (1985) 169.
[22] K. Nakamoto, Infrared and Raman Spectra of Inorganic and Coordination Compounds, Wiley, New York, 1978.
[23] G. Domazetis, R.J. Megee, B.D. James, J. Organomet. Chem. 173 (1979) 357.
[24] R.M. Silverstein, O.G. Bassler, T.C. Morrill, Spectrophotometic Identification of Organic Compounds, Wiley, NewYork, 1974.
[25] H. Shindo, T.L. Brown, J. Am. Chem. Soc. 87 (1965) 1904.
[26] A. Bravo, J.R. Anacona, Trans. Met. Chem. 26 (2001) 20.
[27] G.B. Deacon, R.J. Phillips, Coord. Chem. Rev. 33 (1980) 227.
[28] G.B. Deacon, F. Huber, R.J. Phillips, Inorg. Chim. Acta 104 (1985) 41.
[29] C.C. Addison, D. Sultons, Prog. Inorg. Chem. 8 (1967) 195.
[30] C.C. Addison, N. Logan, S.C. Wallwork, C.D. Garner, Quart. Rev. Chem. Soc. 25 (1971) 289.
[31] A.B.P. Lever, E. Manto Vani, B.S. Ramaswami, Can. J. Chem. 49 (1971) 1957.
[32] M. Choca, J.R. Ferraro, K. Nakamoto, J. Chem. Soc. A (1972) 2297.
[33] P.L. Goggin, R.J. Goodfellow, J. Chem. Soc. A (1966) 1462.
[34] W.J. Barreto, H.D. Santana, F.A.S. Almeida, D.N. Ishikawa, Y. Kawano, J. Anal. Appl. Pyrol. 70 (2003) 199.
[35] B.N. Figgis, Introduction to Ligand Fields, 1st ed., 1966.
[36] A.B.P. Lever, Inorganic Electronic Spectroscopy, Elsevier, Amsterdam, 1968.
[37] K. Nakamoto, S.J. McCarthy, Spectroscopy and structure of Metal Chelate Compounds, John Wiley and Sons, USA, 1968.
[38] E.S. Freeman, B. Carroll, J. Phys. Chem. 62 (1958) 394.
[39] J. Sestak, V. Satava, W. Wendlandt, Thermochim. Acta 7 (1973) 333.
[40] A.W. Coats, J.P. Redfern, Nature 68 (1964) 201.
[41] T. Ozawa, Bull. Chem. Soc. Jpn. 38 (1965) 1881.
[42] W.W. Wendlandt, Thermal Methods of Analysis, Wiley, New York, 1974.
[43] H.W. Horowitz, G. Metzger, Anal. Chem. 35 (1963) 1464.
[44] J.H. Flynn, A. Wall, Polym. Lett. 4 (1966) 323.
[45] R. Shirley, The CRYSFIRE System for Automatic Powder Indexing: Users Manual, Lattice Press, 2002.